Mineralogical Magazine (2021), **85**, 698–707
doi:10.1180/mgm.2021.47

CAMBRIDGE UNIVERSITY PRESS

Article

New arsenate minerals from the Arsenatnaya fumarole, Tolbachik volcano, Kamchatka, Russia. XVI. Yurgensonite, $K_2SnTiO_2(AsO_4)_2$, the first natural tin arsenate, and the katiarsite–yurgensonite isomorphous series

Igor V. Pekov[1]*, Natalia V. Zubkova[1], Atali A. Agakhanov[2], Vasiliy O. Yapaskurt[1], Dmitry I. Belakovskiy[2], Marina F. Vigasina[1], Sergey N. Britvin[3], Anna G. Turchkova[1], Evgeny G. Sidorov[4,†] and Dmitry Yu. Pushcharovsky[1]

[1]Faculty of Geology, Moscow State University, Vorobievy Gory, 119991 Moscow, Russia; [2]Fersman Mineralogical Museum of the Russian Academy of Sciences, Leninsky Prospekt 18-2, 119071 Moscow, Russia; [3]Department of Crystallography, St. Petersburg State University, University Emb. 7/9, 199034 St. Petersburg, Russia; and [4]Institute of Volcanology and Seismology, Far Eastern Branch of Russian Academy of Sciences, Piip Boulevard 9, 683006 Petropavlovsk-Kamchatsky, Russia

Abstract

The new mineral yurgensonite, ideally $K_2SnTiO_2(AsO_4)_2$, the first natural arsenate with species-defining tin, and the continuous isomorphous series between yurgensonite and katiarsite $KTiO(AsO_4)$ are described from sublimates of the Arsenatnaya fumarole at the Second scoria cone of the Northern Breakthrough of the Great Tolbachik Fissure Eruption, Tolbachik volcano, Kamchatka, Russia. Yurgensonite and a Sn-bearing variety of katiarsite are associated closely with one another and with badalovite, pansnerite, yurmarinite, achyrophanite, arsenatrotitanite, hatertite, khrenovite, svabite, sanidine, hematite, cassiterite, rutile and aphthitalite-group sulfates. Yurgensonite occurs as sword-shaped crystals up to 0.01 mm × 0.05 mm × 1 mm or acicular to hair-like individuals up to 1 mm long, typically forming radial aggregates up to 2 mm across. It is transparent, colourless, white or pale beige, with vitreous lustre. The mineral is brittle, cleavage was not observed. D_{calc} is 3.877 g cm^{-3}. Yurgensonite is optically biaxial (–), $\alpha = 1.764(6)$, $\beta = 1.780(6)$, $\gamma = 1.792(6)$ and $2V_{meas.}$ is large. Chemical composition (wt.%, electron-microprobe; holotype) is: Na_2O 0.51, K_2O 16.27, Rb_2O 0.12, Al_2O_3 0.26, Fe_2O_3 4.33, SiO_2 0.29, TiO_2 10.17, SnO_2 22.01, P_2O_5 0.14, V_2O_5 0.19, As_2O_5 40.20, Sb_2O_5 4.88, SO_3 0.28, total 99.65. The empirical formula based on 10 O apfu is $(K_{1.92}Na_{0.09}Rb_{0.01})_{\Sigma 2.02}(Sn_{0.81}Ti_{0.71}Fe^{3+}_{0.30}Sb^{5+}_{0.17}Al_{0.03})_{\Sigma 2.02}(As_{1.945}Si_{0.03}S_{0.02}P_{0.01}V_{0.01})_{\Sigma 2.015}O_{10}$. Yurgensonite is orthorhombic, $Pna2_1$, $a = 13.2681(6)$, $b = 6.6209(3)$, $c = 10.8113(5)$ Å, $V = 949.74(7)$ Å^3 and $Z = 4$. The crystal structure was solved from single-crystal X-ray diffraction data, $R = 5.02\%$. Yurgensonite belongs to the KTP-structure type. It is a Ti,Sn-ordered analogue of katiarsite. The structure contains chains of corner-linked alternating crystallographically non-equivalent octahedra $M(1)$ and $M(2)$. In yurgensonite, Sn^{4+} prevails in the $M(2)O_6$ octahedron whereas the $M(1)$ site is Ti^{4+}-dominant. The new mineral is named in honour of the Russian mineralogist, geochemist and specialist in studies of ore deposits Professor Georgiy Aleksandrovich Yurgenson (born 1935).

Keywords: yurgensonite, new mineral, katiarsite, potassium titanium tin arsenate, isomorphism of tin and titanium, crystal structure, KTP structure type, fumarole sublimate, Tolbachik volcano, Kamchatka

(Received 29 January 2021; accepted 25 May 2021; Accepted Manuscript published online: 28 May 2021; Associate Editor: Koichi Momma)

Introduction

This paper continues the series of articles devoted to new arsenate minerals discovered in the active Arsenatnaya fumarole located at the apical part of the Second scoria cone of the Northern Breakthrough of the Great Tolbachik Fissure Eruption 1975–1976, Tolbachik volcano, Kamchatka Peninsula, Far-Eastern Region, Russia (55°41′N 160°14′E, 1200 m a.s.l.). Eighteen new species were described in previous articles of this series, namely yurmarinite $Na_7(Fe^{3+},Mg,Cu)_4(AsO_4)_6$ (Pekov *et al.*, 2014a), ericlaxmanite and kozyrevskite, two polymorph modifications of $Cu_4O(AsO_4)_2$ (Pekov *et al.*, 2014b), popovite $Cu_5O_2(AsO_4)_2$ (Pekov *et al.*, 2015a), shchurovskyite $K_2CaCu_6O_2(AsO_4)_4$ and dmisokolovite $K_3Cu_5AlO_2(AsO_4)_4$ related to one another in terms of crystal chemistry (Pekov *et al.*, 2015b), katiarsite $KTiO(AsO_4)$ (Pekov *et al.*, 2016a), melanarsite $K_3Cu_7Fe^{3+}O_4(AsO_4)_4$ (Pekov *et al.*, 2016b), pharmazincite $KZnAsO_4$ (Pekov *et al.*, 2017), arsenowagnerite $Mg_2(AsO_4)F$ (Pekov *et al.*, 2018b), arsenatrotitanite $NaTiO(AsO_4)$ (Pekov *et al.*, 2019a), edtollite $K_2NaCu_5Fe^{3+}O_2(AsO_4)_4$ and its Al-dominant analogue alumoedtollite $K_2NaCu_5AlO_2(AsO_4)_4$ (Pekov *et al.*, 2019b), anatolyite $Na_6(Ca,Na)(Mg,Fe^{3+})_3Al(AsO_4)_6$ (Pekov *et al.*, 2019c), zubkovaite $Ca_3Cu_3(AsO_4)_4$ (Pekov *et al.*, 2019d), pansnerite $K_3Na_3Fe^{3+}_6(AsO_4)_8$ (Pekov *et al.*, 2020a), badalovite $NaNaMg(MgFe^{3+})(AsO_4)_3$ (Pekov *et al.*, 2020b) and calciojohillerite $NaCaMgMg_2(AsO_4)_3$ (Pekov *et al.*, 2021).

***Author for correspondence:** Igor V. Pekov, Email: igorpekov@mail.ru
†Deceased 20 March 2021
Cite this article: Pekov I.V., Zubkova N.V., Agakhanov A.A., Yapaskurt V.O., Belakovskiy D.I., Vigasina M.F., Britvin S.N., Turchkova A.G., Sidorov E.G., Pushcharovsky D.Y. (2021) New arsenate minerals from the Arsenatnaya fumarole, Tolbachik volcano, Kamchatka, Russia. XVI. Yurgensonite, $K_2SnTiO_2(AsO_4)_2$, the first natural tin arsenate, and the katiarsite–yurgensonite isomorphous series. *Mineralogical Magazine* **85**, 698–707. https://doi.org/10.1180/mgm.2021.47

In this paper, we characterise the new mineral yurgensonite, ideally $K_2SnTiO_2(AsO_4)_2$, the first natural arsenate with species-defining tin, and the isomorphous series between yurgensonite and katiarsite.

The new mineral is named in honour of the Russian mineralogist, geochemist and specialist in studies of ore deposits Professor Georgiy Aleksandrovich Yurgenson (born 1935), an Honorary member of the Russian Mineralogical Society. He works in the Institute of Natural Resources, Ecology and Cryology of the Siberian Branch of the Russian Academy of Sciences, Chita, Russia. Prof. Yurgenson made a significant contribution to the mineralogy and geochemistry of tin deposits of the Transbaikal Region, South Siberia, and the geochemistry of arsenic in the oxidation zone of ore deposits.

Both the new mineral and its name have been approved by the IMA Commission on New Minerals, Nomenclature and Classification, IMA2019–059 (Pekov *et al.*, 2019e). The type specimens are deposited in the systematic collection of the Fersman Mineralogical Museum of the Russian Academy of Sciences, Moscow with the catalogue numbers 96702 and 96703.

Occurrence and general appearance

The Arsenatnaya fumarole, one of the most strongly mineralised and mineralogically interesting fumaroles at the Tolbachik volcano, has been described, including the data on zonation in distribution of mineral associations, in previous literature (Pekov *et al.*, 2014a, 2018a; Shchipalkina *et al.*, 2020).

All members of the isomorphous series between yurgensonite and katiarsite are minor components of the arsenate mineralisation occurring in the so-called polymineralic zone of the Arsenatnaya fumarole. They were found at a depth of 1–1.5 m from the day surface. Specimens with yurgensonite and a Sn-rich variety of katiarsite were collected by us in July 2018 from the north part of the fumarole. Temperatures measured by us using a chromel–alumel thermocouple in pockets with these minerals at the time of collecting were 360–400°C. Minerals of the katiarsite–yurgensonite series were deposited directly from the gas phase as a volcanic sublimates or, more probably, formed as a result of the interaction between fumarolic gas, an obvious carrier of As, Sn and K, with basalt scoria. The latter could be a source of Ti which has low volatility in volcanic gases, as both thermodynamic calculations (Churakov *et al.*, 2000) and direct measurements carried out for gases of Tolbachik (Zelenski *et al.*, 2014) demonstrate.

Yurgensonite and the Sn-bearing variety of katiarsite are associated closely with one another, with other arsenates, namely badalovite, pansnerite, yurmarinite, achyrophanite, arsenatrotitanite, hatertite, khrenovite and svabite; and with sanidine, hematite, cassiterite (Ti-, Fe^{3+}- and Sb^{5+}-enriched varieties), rutile (Sn-, Fe^{3+}- and Sb^{5+}-enriched varieties) and aphthitalite-group sulfates. Katiarsite–yurgensonite series members overgrow white to yellowish sanidine crusts and yellow- or brownish-green badalovite crystals on the surface of basalt scoria altered by fumarolic gas (Fig. 1).

Yurgensonite occurs as sword-shaped crystals (Figs 1a and 2a) up to 0.01 mm × 0.05 mm × 1 mm or acicular to hair-like individuals (Figs 1b and 2b) up to 1 mm long. They are elongated along [010]; sword-like crystals are flattened on [100]. The major forms of sword-shaped crystals (Fig. 2a) are {100}, {001} (prismatic zone) and {011} (terminations). Acicular individuals are typically split and consist of numerous crystals (subindividuals) (Fig. 2b). Sword-like crystals are commonly combined in parallel or near-parallel intergrowths (Fig. 1a) whereas acicular and hair-like individuals form radial, sheaf- or bush-like aggregates, sprays (Figs 1b and 2b) or open-work rosettes and spherulites up to 2 mm across. The Sn-enriched variety of katiarsite, visually indistinguishable from yurgensonite, also typically forms radial aggregates of acicular to hair-like crystals of the same size (Figs 1c and 2c). Epitactic overgrowing of flattened pansnerite crystals on acicular crystals of katiarsite–yurgensonite series minerals was observed (Fig. 3).

Physical properties

Yurgensonite and a Sn-bearing variety of katiarsite are transparent in individuals and translucent in aggregates. They are colourless, white or pale beige, with white streak and vitreous lustre. Neither mineral fluoresces in UV light. They are brittle, cleavage or parting was not observed. The fracture is uneven. The hardness and density were not measured because crystals are small and thin and aggregates are open-work. Density calculated for the holotype yurgensonite using the empirical formula and unit-cell volume determined from the single-crystal X-ray diffraction (XRD) data is 3.877 g cm^{-3}.

Optical data

In plane polarised transmitted light, yurgensonite is colourless and non-pleochroic. It is optically biaxial (–), $\alpha = 1.764(6)$, $\beta = 1.780(6)$ and $\gamma = 1.792(6)$ (589 nm); $2V_{meas.}$ is large, close to 90°; $2V_{calc.} = 81°$. Dispersion of optical axes is distinct, $r < v$. Optical orientation is: $X = b$, $Y = a$ and $Z = c$.

The increase of the Ti:Sn ratio in the katiarsite–yurgensonite series is accompanied by the increase of all three refractive indices and birefringence (Table 1). Yurgensonite and katiarsite demonstrate the same feature as other known pairs of isostructural minerals with Ti^{4+} and Sn^{4+}: the titanium member of such a pair has significantly higher refractive indices than the tin member (Table 2). Thus, despite a much higher atomic number of tin (50) and, thus, number of electrons in comparison with titanium (atomic number 22), Ti^{4+} compounds have higher refractive indices than isostructural Sn^{4+} compounds, apparently caused by significant difference in the electron structure of Ti and Sn atoms. In addition to significant substitution of Ti^{4+} for Sn^{4+}, the Ti–Sn ordering and microtwinning (see below) could cause the difference in optical sign and 2V value between katiarsite and yurgensonite (Table 1).

Raman spectroscopy

The Raman spectrum of yurgensonite (Fig. 4) was obtained on an aggregate of randomly oriented acicular crystals using an EnSpectr R532 instrument with a green laser (532 nm) at room temperature. The output power of the laser beam was ~14 mW. The spectrum was processed using the *EnSpectr* expert mode program in the range from 100 to 4000 cm^{-1} with the use of a holographic diffraction grating with 1800 lines cm^{-1} and a resolution of 6 cm^{-1}. The diameter of the focal spot on the sample was ~25 μm. The back-scattered Raman signal was collected with 40× objective; signal acquisition time for a single scan of the spectral range was 2000 ms and the signal was averaged over 6 scans.

Bands in the region between 740 and 900 cm^{-1} in the Raman spectrum of yurgensonite correspond to As^{5+}–O antisymmetric stretching vibrations of AsO_4 groups. A broad band with the main maximum at 648 cm^{-1} can be assigned to Ti–O and Sn–O

https://doi.org/10.1180/mgm.2021.47 Published online by Cambridge University Press

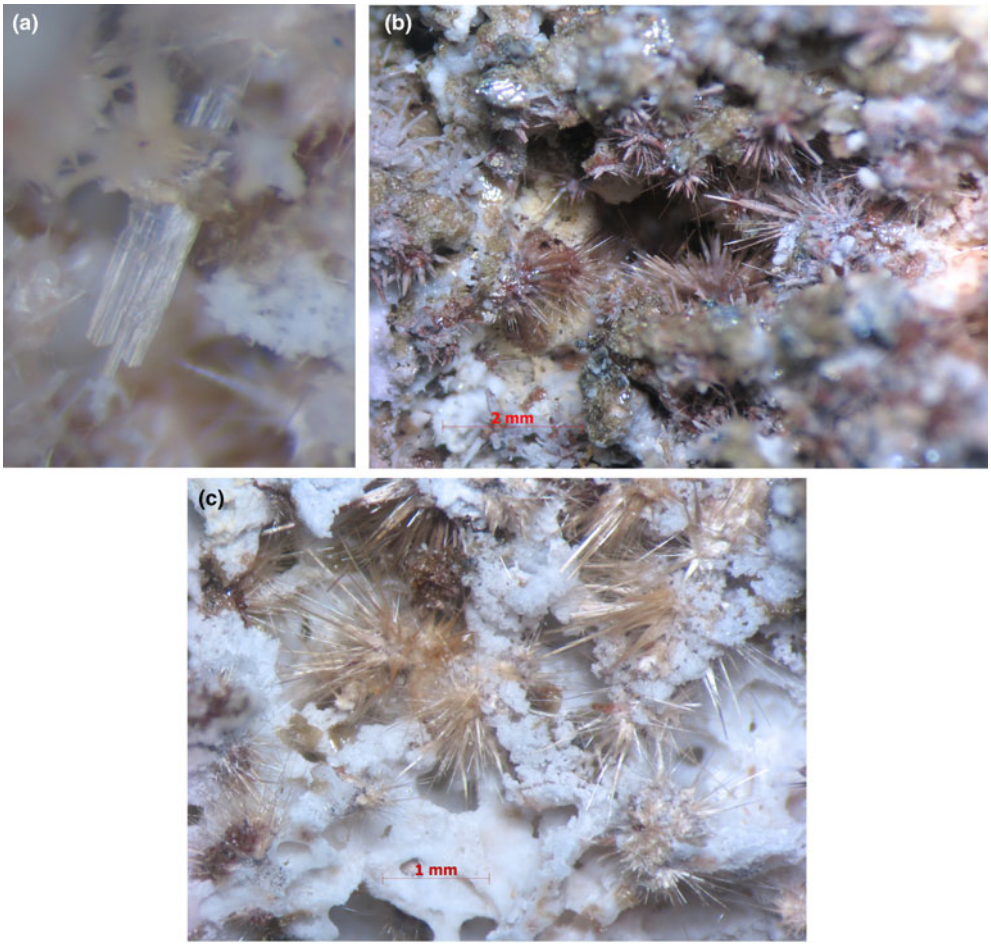

Fig. 1. Morphology of yurgensonite (a, b) and Sn-rich variety of katiarsite (c): (a) parallel intergrowth of three sword-shaped transparent colourless yurgensonite crystals with white sanidine; (b) numerous sprays of colourless acicular yurgensonite crystals, partially overgrown by reddish-brown pansnerite and milky-white aphthitalite, on aggregates of yellowish sanidine and light brownish-green badalovite; (c) numerous bush-like clusters of beige acicular crystals of Sn-rich katiarsite on white sanidine crust. The figure (a) shows the holotype specimen of yurgensonite. FOV width: (a) 0.75 mm, (b) 9 mm, (c) 5.8 mm. Photo: I.V. Pekov and A.V. Kasatkin.

stretching vibrations in MO_6 octahedra (see below). A strong band at 484 cm^{-1} (with distinct low-frequency shoulder) probably corresponds to stretching vibrations of non-bridging Ti–O/Sn–O bonds and antisymmetric vibrations of Ti–O–Sn/Ti–O–Ti/Sn–O–Sn bridges. Bands with frequencies lower than 400 cm^{-1} correspond to lattice modes involving As–O, Sn–O and Ti–O bending and K–O stretching vibrations. The bands in the spectrum are assigned according to Nakamoto (1986) and Watson (1991).

The Raman spectrum of yurgensonite is, in general, similar to the spectra of katiarsite (Pekov *et al.*, 2016a) and its synthetic analogue KTA (Watson, 1991). However, all bands with frequencies lower than 740 cm^{-1} (i.e. involving vibrations in octahedra) in the spectrum of the new mineral are shifted to lower frequencies in comparison with katiarsite, due to the substitution of ~50% of Ti^{4+} for the heavier and larger Sn^{4+} cation in yurgensonite.

The absence of bands with frequencies higher than 900 cm^{-1} indicates the absence of groups with O–H, C–H, C–O, N–H, N–O and B–O bonds in yurgensonite.

Chemical composition

The chemical composition of the katiarsite–yurgensonite series minerals was determined in two laboratories. In the Fersman Mineralogical Museum (FMM), the minerals were studied using a Jeol 733 electron microprobe instrument and in the Laboratory of Analytical Techniques of High Spatial Resolution, Dept. of Petrology, Moscow State University (MSU), a Jeol JSM-6480LV scanning electron microscope equipped with an INCA-Wave 500 wavelength-dispersive spectrometer was used. In both cases WDS mode was used, with an acceleration voltage of 20 kV, a beam current of 20 nA and a 3 μm beam diameter. The following standards were used (FMM / MSU): Na (albite / albite), K (microcline / microcline), Rb ($Rb_2Nb_4O_{11}$ / $Rb_2Nb_4O_{11}$), Cu (Cu metal/ Cu metal), Al (Al_2O_3 / Al_2O_3), Fe (InAs / FeAsS), Si (microcline / diopside), Ti (ilmenite / $MnTiO_3$), Sn (SnO_2 / SnS), P ($LaPO_4$ / GaP), V (V metal / V metal), As (InAs / FeAsS), Sb (Sb / Sb_2S_3) and S (ZnS / ZnS). Contents of other elements with atomic numbers higher than carbon are below detection limits.

A representative selection of electron-microprobe analyses of minerals belonging to the katiarsite–yurgensonite series are given in Table 3 and the ratios of the major octahedrally coordinated components in these arsenates are shown in Fig. 5.

The empirical formula of the holotype yurgensonite (#11 in Table 3) calculated on the basis of 10 O atoms per formula unit (apfu) is $(K_{1.92}Na_{0.09}Rb_{0.01})_{\Sigma 2.02}(Sn_{0.81}Ti_{0.71}Fe^{3+}_{0.30}Sb^{5+}_{0.17}Al_{0.03})_{\Sigma 2.02}(As_{1.945}Si_{0.03}S_{0.02}P_{0.01}V_{0.01})_{\Sigma 2.015}O_{10}$. The idealised formula, written taking into account the ordering of Sn and Ti (see below), is $K_2SnTiO_2(AsO_4)_2$.

https://doi.org/10.1180/mgm.2021.47 Published online by Cambridge University Press

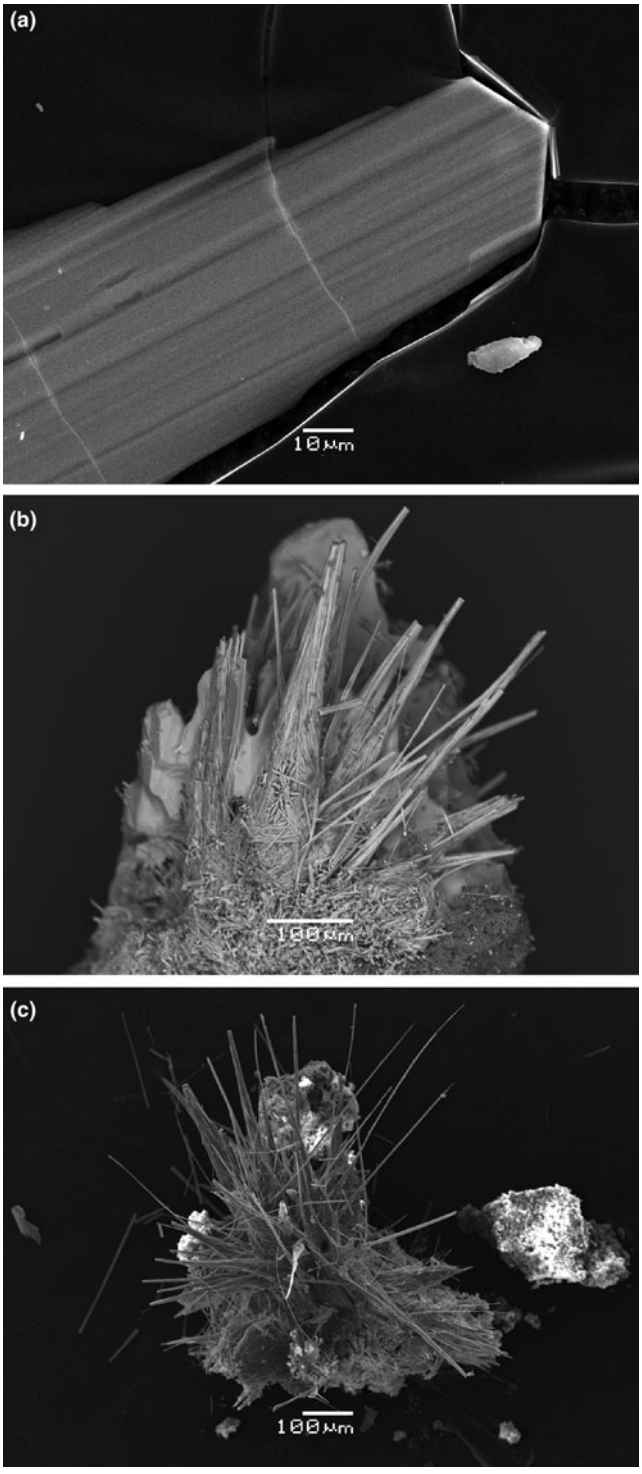

Fig. 2. Morphology of yurgensonite (a, b) and Sn-rich variety of katiarsite (c): (a) sword-shaped yurgensonite crystal extracted from the holotype specimen; (b) bush-like aggregate of acicular yurgensonite individuals (some of them are split and consist of numerous sub-individuals) on crude crystals of badalovite; (c) bush-like aggregate of acicular to hair-like individuals of Sn-rich katiarsite on sanidine. Scanning electron microscopy images, secondary electron (a, c) and back-scattered electron (b) modes.

Iron is the major admixed component in katiarsite–yurgensonite series minerals: all the samples studied contain from 3.3 to 5.4 wt.% Fe_2O_3 that corresponds to 0.2–0.35 Fe apfu. Antimony can be a significant admixture: in some samples, up to 6.0 wt.% Sb_2O_5 was found (up to 0.2 Sb apfu); however, other samples are Sb-free. Both Fe and Sb seem to be the constituents which substitute Ti and/or Sn at the octahedrally coordinated *M* sites (see below), as well as minor Al and Cu. Unlike iron, for which the content does not depend on the Ti:Sn ratio in minerals of this series, antimony is mainly concentrated in tin-rich samples (Table 3). Among tetrahedrally coordinated components *T*, arsenic strongly prevails: the contents of admixed V, P, S and Si together do not exceed 0.13 apfu (#9 in Table 3). Large cations *A* are represented mainly by potassium whereas admixed sodium content is up to 0.25 apfu = 1.5 wt.% Na_2O (#5 in Table 3).

Fig. 3. Parallel intergrowths of acicular yurgensonite crystals (white) epitaxially overgrown by elongated tabular crystals of pansnerite $K_3Na_3Fe^{3+}_6(AsO_4)_8$ (light grey). Back-scattered electron image.

Table 1. Comparative data of katiarsite and yurgensonite, two natural representatives of the KTP-structure type.

Mineral	Katiarsite	Yurgensonite
Ideal formula	$KTiO(AsO_4)$	$K_2SnTiO_2(AsO_4)_2$
Crystal system	Orthorhombic	Orthorhombic
Space group	$Pna2_1$	$Pna2_1$
a (Å)	13.174(4)	13.2681(6)
b (Å)	6.5635(10)	6.6209(3)
c (Å)	10.805(2)	10.8113(5)
V (Å^3)	934.3(3)	949.74(7)
Z	8	4
Strongest reflections of the powder X-ray diffraction pattern: *d*, Å – *I*	5.91 – 17 5.62 – 74 3.157 – 66 2.826 – 100 2.809 – 96 2.704 – 19	5.930 – 16 5.656 – 100 3.171 – 50 2.861 – 49 2.830 – 82 2.707 – 17
D (calc.) g cm^{-3}	3.49	3.88
Optical data:	Biaxial (+)	Biaxial (–)
α	1.784	1.764
β	1.792	1.780
γ	1.870	1.792
$2V_{calc.}$	37°	81°
Birefringence	0.086	0.028
Source	Pekov *et al.* (2016a)	this work

X-ray crystallography and crystal structure determination

Powder XRD data of the holotype yurgensonite (Table 4) were collected with a Rigaku R-AXIS Rapid II single-crystal

https://doi.org/10.1180/mgm.2021.47 Published online by Cambridge University Press

Table 2. Refractive indices of isostructural Sn^{4+} and Ti^{4+} minerals.

Minerals / formulae	α / ω or ε	β	γ / ε or ω	Source
Cassiterite / SnO_2	1.99–2.01		2.09–2.10	Anthony *et al.* (1990b)
Rutile / TiO_2	2.605–2.613		2.90	Anthony *et al.* (1990b)
Malayaite / $CaSnO(SiO_4)$	1.764–1.765	1.783–1.786	1.798–1.801	Anthony *et al.* (1990a)
Titanite / $CaTiO(SiO_4)$	1.843–1.950	1.830–2.034	1.943–2.11	Anthony *et al.* (1990a)
Pabstite / $BaSn(Si_3O_9)$	1.674		1.685	Anthony *et al.* (1990a)
Benitoite / $BaTi(Si_3O_9)$	1.756–1.757		1.802–1.804	Anthony *et al.* (1990a)
Brannokite / $KLi_3Sn_2(Si_{12}O_{30})$	1.566		1.567	Anthony *et al.* (1990a)
Berezanskite / $KLi_3Ti_2(Si1_2O_{30})$	1.630		1.635	Pautov and Agakhanov (1997)
Yurgensonite / $K_2SnTiO_2(AsO_4)_2$	1.764	1.78	1.792	this work
Katiarsite / $KTiO(AsO_4)$	1.784	1.792	1.870	Pekov *et al.* (2016a)

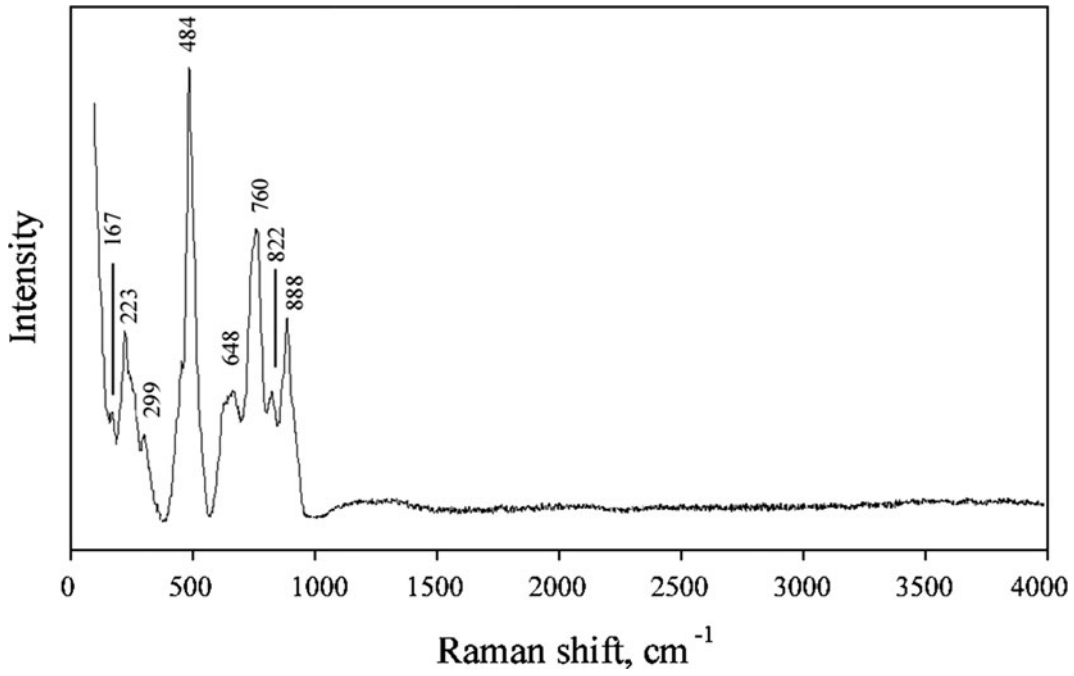

Fig. 4. The Raman spectrum of yurgensonite.

diffractometer equipped with cylindrical image plate detector (radius 127.4 mm) using Debye-Scherrer geometry, Co*K*α radiation (rotating anode with VariMAX microfocus optics), 40 kV, 15 mA and exposure 15 min. Angular resolution of the detector is 0.045°2θ (pixel size 0.1 mm). The data were integrated using the software package *osc2Tab* (Britvin *et al.*, 2017). Parameters of the orthorhombic unit cell calculated from the powder data are: $a = 13.276(3)$, $b = 6.629(2)$, $c = 10.823(4)$ Å and $V = 952.5(8)$ Å^3.

Powder XRD patterns of yurgensonite and Sn-free katiarsite (Pekov *et al.*, 2016a) are very close, the difference is only in values of *d* spacings which are smaller for the latter (Table 1).

The powder XRD pattern of a Ti-rich variety of yurgensonite was obtained under the same conditions (specimen chemically close to the border with katiarsite: #9 in Table 3). It is very similar to the patterns of Sn-free katiarsite (Pekov *et al.*, 2016a) and the Sn-rich variety of yurgensonite (holotype: Table 4); in comparison with them, this intermediate in the Ti:Sn ratio sample demonstrates intermediate *d* spacings. Its unit-cell parameters calculated from the powder data are: $a = 13.178(8)$, $b = 6.583(2)$, $c = 10.826(7)$ Å and $V = 939(1)$ Å^3.

Single-crystal XRD studies of the holotype yurgensonite were carried out using an Xcalibur S diffractometer equipped with a CCD detector. A full sphere of three-dimensional data was collected. Crystal data, data collection information and structure refinement details are given in Table 5. Data reduction was performed using *CrysAlisPro* Version 1.171.37.35 (Agilent, 2014). The data were corrected for Lorentz and polarisation effects. The structure was solved by direct methods and refined with the use of *SHELX* software package (Sheldrick, 2015) on the basis of 2235 independent reflections with $I > 2\sigma(I)$ to the final $R = 0.0502$. The twinning by merohedry Class I (Nespolo and Ferraris, 2000) with an inversion centre as a twinning operator was found in the crystal studied. The twin domains ratio is 54/46. Atom coordinates and displacement parameters are presented in Table 6, selected interatomic distances in Table 7 and bond valence calculations in Table 8. The crystallographic information file has been deposited with the Principal Editor of *Mineralogical Magazine* and is available as Supplementary material (see below).

Discussion

Yurgensonite $K_2SnTiO_2(AsO_4)_2$ is a Ti,Sn-ordered isostructural analogue of katiarsite $KTiO(AsO_4)$ (Table 1). Both minerals, found only in the Arsenatnaya fumarole, are representatives of

https://doi.org/10.1180/mgm.2021.47 Published online by Cambridge University Press

Table 3. Chemical composition of minerals of the katiarsite–yurgensonite isomorphous series.

No	1	2 ht	3	4	5	6	7	8	9	10	11 ht	12	13	14
Wt. %														
Na_2O		-	0.62	1.05	1.50	0.61	0.46	1.32	0.88	0.43	0.51 (0.4–0.6)	0.47	0.57	
K_2O	19.47	18.98	18.12	17.38	16.41	17.51	17.26	16.08	16.33	16.31	16.27 (16.0–16.5)	16.27	16.02	16.98
Rb_2O		-	-	-	-	-	-	-	-	0.12	0.12 (0.05–0.2)	0.22	0.06	
CuO		-	-	-	0.45	-	0.63	-	0.86	-	-	-	-	
Al_2O_3		-	0.49	-	0.26	0.48	0.35	0.36	-	0.40	0.26 (0.2–0.4)	0.18	0.20	
Fe_2O_3		5.07	4.08	3.98	5.40	4.19	4.36	4.91	4.09	3.62	4.33 (3.3–5.2)	5.23	3.35	
SiO_2		-	0.34	0.22	-	-	-	-	-	0.22	0.29 (0.1–0.6)	0.13	0.24	
TiO_2	33.03	27.49	24.97	23.24	19.66	19.59	16.62	16.28	15.01	12.15	10.17 (8.8–12.2)	8.77	10.28	14.41
SnO_2		-	4.79	8.10	9.06	12.87	12.92	13.29	14.87	20.70	22.01 (20.2–24.0)	23.06	24.04	27.17
P_2O_5		-	0.60	0.61	0.17	0.63	0.39	0.77	0.48	0.26	0.14 (0.1–0.3)	0.13	0.10	
V_2O_5		-	-	0.50	0.39	-	0.45	-	1.23	-	0.19 (0.00–0.4)	0.41	-	
As_2O_5	47.50	47.48	44.91	43.96	44.02	44.17	42.22	43.37	41.61	40.19	40.20 (39.6–41.0)	39.63	40.01	41.44
Sb_2O_5		-	-	-	1.02	0.78	3.35	4.01	4.84	4.81	4.88 (4.0–6.0)	3.99	4.67	
SO_3		-	0.12	0.09	0.28	-	0.24	-	0.29	-	0.28 (0.00–0.5)	0.52	0.33	
Total	100	99.02	99.04	99.13	99.10*	100.83	99.25	100.39	100.49	99.21	99.65	99.01	99.87	100
Atoms per formula unit based on 10 O														
Na		-	0.10	0.17	0.25	0.10	0.08	0.22	0.15	0.08	0.09	0.09	0.10	
K	2	2.00	1.93	1.88	1.80	1.91	1.95	1.79	1.84	1.92	1.92	1.95	1.90	2
Rb		-	-	-	-	-	-	-	-	0.01	0.01	0.01	0.00	
Cu		-	-	-	0.03	-	0.04	-	0.06	-	-	-	-	
Al		-	0.05	-	0.03	0.05	0.04	0.04	-	0.04	0.03	0.02	0.02	
Fe^{3+}		0.32	0.26	0.25	0.35	0.27	0.29	0.32	0.27	0.25	0.30	0.37	0.23	
Ti	2	1.70	1.57	1.48	1.27	1.26	1.11	1.07	0.99	0.84	0.71	0.62	0.72	1
Sn^{4+}		-	0.16	0.27	0.31	0.44	0.45	0.46	0.52	0.76	0.81	0.86	0.89	1
Sb^{5+}		-	-	-	0.03	0.02	0.11	0.13	0.16	0.16	0.17	0.14	0.16	
Si		-	0.03	0.02	-	-	-	-	-	0.02	0.03	0.01	0.02	
P		-	0.04	0.04	0.01	0.05	0.03	0.06	0.04	0.02	0.01	0.01	0.01	
V^{5+}		-	-	0.03	0.02	-	0.03	-	0.07	-	0.01	0.03	-	
As^{5+}	2	2.04	1.96	1.94	1.98	1.97	1.95	1.97	1.92	1.94	1.945	1.94	1.94	2
S^{6+}		-	0.01	0.01	0.02	-	0.02	-	0.02	-	0.02	0.04	0.02	

1–8 – katiarsite [1 – calculated values for $KTiO(AsO_4)$; 2 ht – holotype specimen: Pekov *et al.*, 2016a], 9–14 – yurgensonite [11 ht – holotype specimen, averaged values for four spot analyses, ranges are in parentheses; 14 – calculated values for $K_2SnTiO_2(AsO_4)_2$]. Analyses are ordered by increase of Sn content. Dash means that the content of a constituent is below detection limit. *Total also includes 0.48 wt.% Nb_2O_5 that corresponds to 0.02 Nb apfu.

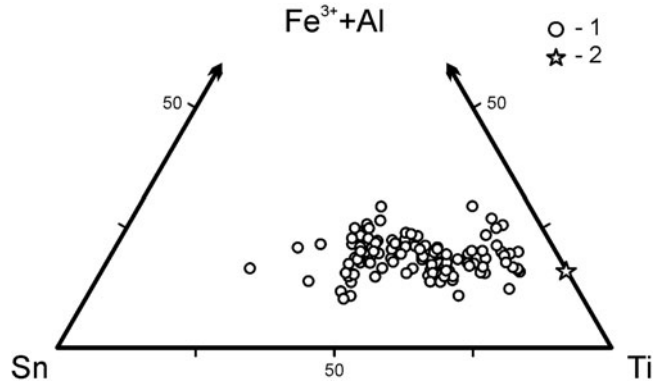

Fig. 5. Ratios of major octahedrally coordinated cations (M) in minerals of the katiarsite–yurgensonite series: 1 – this work, 2 – holotype katiarsite (Pekov *et al.*, 2016a).

the well-known KTP [$KTiO(PO_4)$] structure type. The KTP family contains more than forty isostructural ($Pna2_1$) synthetic phosphates and arsenates with the general formulae $A^+M^{4+}O(T^{5+}O_4)$ [T^{5+} = P and As; M^{4+} = Ti, Ge, V, Sn, Zr, ($Ga^{3+}_{0.5}Nb^{5+}_{0.5}$), ($Fe^{3+}_{0.5}Nb^{5+}_{0.5}$), ($Mn^{3+}_{0.5}Nb^{5+}_{0.5}$) and ($Mg^{2+}_{0.33}Nb^{5+}_{0.67}$); A^+ = K, Na, Rb, Cs, Ag, NH_4 and Tl] and $KM^{3+}(F,OH)(T^{5+}O_4)$ [T^{5+} = P and As; M^{3+} = Ga and Fe]. Some representatives of this family belong to very important optical crystalline materials. They are unique in overall qualifications for second-order non-linear and electro-optic processes with a large hyperpolarisability, an excellent temperature window, a wide wavelength range for phase matching, and outstanding crystal stability. Some members of this family are characterised by the unique combination of high non-linear susceptibility and ferroelectric superionic conductivity (Novikova *et al.*, 2018).

The crystal structure of KTP-type compounds (see, e.g. Fig. 6) contains undulating chains of corner-linked alternating crystallographically non-equivalent octahedra $M(1)$ and $M(2)$. The chains are cross-linked by TO_4 tetrahedra and thus a heteropolyhedral framework is formed. The A^+ cations occupy the channels of the framework (Stucky *et al.*, 1989; Phillips *et al.*, 1992; Northrup *et al.*, 1994; Weber, 2003).

Yurgensonite is the second mineral belonging to the KTP-structure type, after katiarsite (Pekov *et al.*, 2016a) which is a natural analogue of synthetic compound KTA, one of the most important non-linear optical materials (Mayo *et al.*, 1994; Northrup *et al.*, 1994; Weber, 2003). In yurgensonite, Sn^{4+} prevails in one of two crystallographically non-equivalent octahedrally coordinated sites [$M(2)$] while another octahedron $M(1)O_6$ is Ti^{4+}-dominant (Tables 6 and 7). Potassium cations occupy two sites in the channels of the Sn–Ti–As–O heteropolyhedral framework (Fig. 6). The crystal chemical formula of yurgensonite could be also written in the form $K_2(SnO)(TiO)(AsO_4)_2$.

Crystal structures and physical properties of synthetic KTP-type phosphates in which Ti^{4+} is completely or partially substituted by Sn^{4+} are well-studied and, in particular, a continuous solid-solution series $KTi_{1-x}Sn_xOPO_4$ has been reported (Krotova *et al.*, 2003 and references therein). The compounds with approximately equal contents of Ti and Sn, namely $KTi_{0.47}Sn_{0.53}OPO_4$

https://doi.org/10.1180/mgm.2021.47 Published online by Cambridge University Press

Table 4. Powder X-ray diffraction data (*d* in Å) of yurgensonite.

I_{obs}	I_{calc}*	d_{obs}	d_{calc}**	*h k l*
9	16	6.64	6.634	200
16	19	**5.930**	5.924	110
100	66, 100	**5.656**	5.654, 5.646	201, 011
1	1	5.400	5.406	002
1	2	5.201	5.195	111
4	6	4.305	4.300	211
4	3	4.195	4.191	202
2	2	3.998	3.993	112
10	14	3.679	3.678	310
4	14	3.543	3.541	212
5	19	3.487	3.482	311
50	7, 41, 51	**3.171**	3.171, 3.167, 3.165	401, 203, 013
11	10, 2	3.082	3.079, 3.079	121, 113
3	2	2.967	2.962	220
49	68, 41	**2.861**	2.860, 2.857	411, 221
82	50, 65	**2.830**	2.827, 2.823	402, 022
17	27	**2.707**	2.703	004
14	15	**2.600**	2.598	222
5	4, 3	2.578	2.574, 2.574	321, 313
2	2	2.446	2.441	403
6	14, 5	2.293	2.290, 2.288	421, 223
9	17	2.243	2.241	512
3	2, 1	2.181	2.178, 2.177	314, 130
3	5	2.128	2.135	323
3	2, 5	2.097	2.095, 2.094	404, 024
6	1, 3, 4, 6	2.058	2.059, 2.056, 2.056, 2.055	611, 231, 205, 015
10	2, 4	2.041	2.047, 2.034	602, 521
3	5	2.022	2.019	132
2	2, 4	1.971	1.975, 1.964	330, 423
1	2	1.944	1.943	331
3	3, 6	1.885	1.885, 1.882	603, 033
3	2	1.866	1.864	315
2	4	1.855	1.855	332
3	5	1.841	1.839	620
4	1, 5	1.822	1.822, 1.821	710, 514
4	3	1.815	1.813	621
3	5, 4	1.798	1.797, 1.795	711, 523
10	27	1.773	1.770	424
7	11, 7	1.748	1.747, 1.746	415, 225
3	3	1.736	1.732	333
3	9, 1	1.698	1.697, 1.695	530, 134
7	7, 7	1.658	1.659, 1.655	800, 040
3	4	1.639	1.637	433
2	6, 1	1.627	1.626, 1.624	721, 141
2	4	1.607	1.606	240
9	2, 4, 4, 8, 1, 10	1.586	1.589, 1.589, 1.586, 1.583, 1.583, 1.583	425, 241, 802, 406, 042, 026
2	2, 2, 2	1.540	1.545, 1.539, 1.539	035, 242, 226
1	5	1.522	1.520	624
3	2, 2, 4, 6	1.507	1.511, 1.504, 1.504, 1.504	714, 235, 207, 017
1	2	1.484	1.483	820
3	6, 1, 5	1.469	1.469, 1.467, 1.467	821, 441, 243
1	5	1.456	1.454	516
5	3, 13	1.439	1.439, 1.437	910, 534
3	3, 3, 4	1.431	1.433, 1.430, 1.428	633, 822, 442
2	3, 1	1.400	1.400, 1.397	435, 606
2	3, 3, 1	1.391	1.393, 1.390, 1.388	715, 732, 136
2	5	1.383	1.381	244

*For the calculated pattern, only reflections with intensities ≥1 are given; **for the unit-cell parameters calculated from single-crystal data. The strongest reflections are marked in boldtype.

Table 5. Crystal data, data collection information and structure refinement details for yurgensonite.

Crystal data	
Formula	$K_2(Ti_{0.67}Sn_{0.33})(Sn_{0.64}Ti_{0.36})O_2(AsO_4)_2$
Formula weight	551.98
Temperature (K)	293(2)
Radiation and wavelength (Å)	Mo*Kα*; 0.71073
Crystal system, space group, *Z*	Orthorhombic, *Pna*2_1, 4
Unit cell dimensions (Å/°)	*a* = 13.2681(6), *b* = 6.6209(3), *c* = 10.8113(5)
V (Å^3)	949.74(7)
Absorption coefficient μ, (mm^{-1})	11.235
F_{000}	1020
Data collection	
Crystal size, mm	0.01 × 0.11 × 0.24
Diffractometer	Xcalibur S CCD
θ range for data collection (°) / Collection mode	3.071–28.268 / full sphere
Index ranges	$-17 \le h \le 17$, $-8 \le k \le 8$, $-14 \le l \le 14$
Reflections collected	14,841
Independent reflections	2348 (R_{int} = 0.0666)
Independent reflections with $I > 2\sigma(I)$	2235
Refinement	
Data reduction	*CrysAlisPro*, Agilent Technologies, v. 1.171.37.35 (Agilent, 2014)
Absorption correction	Gaussian [numerical absorption correction based on Gaussian integration over a multifaceted crystal model] Empirical absorption correction using spherical harmonics, implemented in *SCALE3 ABSPACK* scaling algorithm.
Structure solution	Direct methods
Refinement method	Full-matrix least-squares on F^2
Number of refined parameters	108
Final *R* indices [$I > 2\sigma(I)$]	R_1 = 0.0502, wR_2 = 0.1042
R indices (all data)	R_1 = 0.0527, wR_2 = 0.1054
GoF	1.175
Largest diff. peak and hole (e^-/Å^3)	3.16 and −1.28

Table 6. Coordinates and equivalent displacement parameters (U_{eq}, in Å^2) of atoms and site occupancy factors (s.o.f.) for yurgensonite.

Site	*x*	*y*	*z*	U_{eq}	s.o.f.
K(1)	0.3772(4)	0.7783(7)	0.3116(6)	0.0472(13)	1
K(2)	0.1081(3)	0.6963(7)	0.0689(5)	0.0381(11)	1
As(1)	0.49840(12)	0.33027(17)	0.2532(2)	0.0077(3)	1
As(2)	0.17936(8)	0.5060(2)	0.5005(3)	0.0089(3)	1
M(1)	0.37474(9)	0.5034(3)	0.0004(3)	0.0083(4)	$Ti_{0.673(8)}Sn_{0.327(8)}$*
M(2)	0.24689(10)	0.2556(2)	0.24904(19)	0.0082(3)	$Sn_{0.636(8)}Ti_{0.364(8)}$*
O(1)	0.9861(9)	0.0053(17)	0.1334(10)	0.008(3)**	1
O(2)	0.5065(9)	0.466(2)	0.3805(12)	0.018(3)**	1
O(3)	0.3980(8)	0.1798(17)	0.2719(14)	0.017(3)	1
O(4)	0.0977(7)	0.3243(15)	0.2291(11)	0.006(2)	1
O(5)	0.3938(8)	0.8044(16)	0.0380(10)	0.009(2)**	1
O(6)	0.6040(9)	0.7969(18)	0.4787(11)	0.016(3)**	1
O(7)	0.2399(10)	0.043(2)	0.1158(13)	0.016(3)**	1
O(8)	0.2576(9)	0.478(2)	0.3774(12)	0.012(3)**	1
O(9)	0.2198(10)	0.043(2)	0.3726(12)	0.014(3)**	1
O(10)	0.2763(10)	0.457(2)	0.1217(12)	0.012(3)**	1

*Admixed Fe and Sb (see Table 3), close in electron numbers to Ti and Sn, respectively, were not taken into account during refinement; **U_{iso}.

(Krotova *et al.*, 2003), $KTi_{0.5}Sn_{0.5}OPO_4$ (Crennell *et al.*, 1991), $K_{0.5}Na_{0.5}Ti_{0.5}Sn_{0.5}OPO_4$, $Na_{0.5}Rb_{0.5}Ti_{0.5}Sn_{0.5}OPO_4$ and $K_{0.5}Rb_{0.5}Ti_{0.5}Sn_{0.5}OPO_4$ (Crennell *et al.*, 1992), demonstrate significant ordering of Ti and Sn with Ti predominance in the *M*(1) site whereas Sn prevails in *M*(2). For example, the following distribution of Ti and Sn between these sites was found for $KTi_{0.47}Sn_{0.53}OPO_4$: $^{M(1)}(Ti_{0.645}Sn_{0.335})^{M(2)}(Sn_{0.696}Ti_{0.304})$ (Krotova *et al.*, 2003). For $K_{0.5}Rb_{0.5}Ti_{0.5}Sn_{0.5}OPO_4$ the distribution is as follows:

https://doi.org/10.1180/mgm.2021.47 Published online by Cambridge University Press

Table 7. Selected interatomic distances (Å) in the structure of yurgensonite.

K(1)–O(8)	2.640(14)	K(2)–O(1)	2.700(12)
K(1)–O(3)	2.706(13)	K(2)–O(10)	2.795(14)
K(1)–O(2)	2.788(15)	K(2)–O(5)	2.863(12)
K(1)–O(9)	2.805(15)	K(2)–O(7)	2.930(15)
K(1)–O(5)	2.972(12)	K(2)–O(4)	3.014(11)
K(1)–O(1)	3.055(13)	K(2)–O(2)	3.107(14)
K(1)–O(10)	3.244(15)	K(2)–O(3)	3.214(16)
K(1)–O(7)	3.298(16)	K(2)–O(9)	3.278(15)
		K(2)–O(8)	3.309(14)
As(1)–O(2)	1.648(14)	As(2)–O(6)	1.660(12)
As(1)–O(3)	1.676(11)	As(2)–O(7)	1.661(14)
As(1)–O(4)	1.689(10)	As(2)–O(8)	1.699(13)
As(1)–O(1)	1.700(12)	As(2)–O(5)	1.699(11)
<As(1)–O>	1.678	<As(2)–O>	1.680
M(1)–O(10)	1.876(14)	*M*(2)–O(10)	1.957(14)
M(1)–O(9)	1.885(14)	*M*(2)–O(9)	1.973(14)
M(1)–O(6)	2.022(12)	*M*(2)–O(7)	2.016(15)
M(1)–O(5)	2.049(11)	*M*(2)–O(8)	2.030(13)
M(1)–O(2)	2.050(13)	*M*(2)–O(4)	2.042(10)
M(1)–O(1)	2.062(12)	*M*(2)–O(3)	2.082(11)
<*M*(1)–O>	1.991	<*M*(2)–O>	2.017

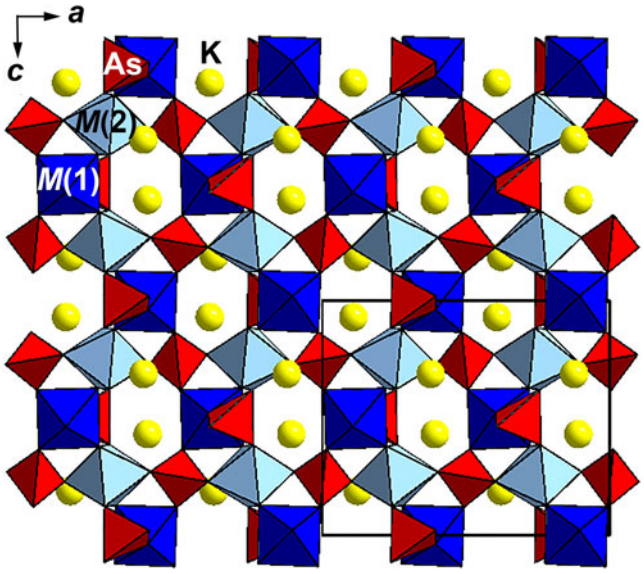

Fig. 6. The crystal structure of yurgensonite projected along the *b* axis. *M*(1) = Ti and *M*(2) = Sn (see Table 6). The unit cell is outlined.

Table 8. Bond valence calculations for yurgensonite.

	K(1)	K(2)	*M*(1)	*M*(2)	As(1)	As(2)	Σ
O(1)	0.08	0.19	0.55		1.20		2.02
O(2)	0.16	0.07	0.57		1.39		2.19
O(3)	0.19	0.05		0.56	1.29		2.09
O(4)		0.09		0.64	1.24		1.97
O(5)	0.10	0.13	0.57			1.21	2.01
O(6)			0.62			1.35	1.97
O(7)	0.04	0.11		0.70		1.34	2.19
O(8)	0.23	0.04		0.66		1.21	2.14
O(9)	0.15	0.05	0.96	0.81			1.97
O(10)	0.05	0.15	0.99	0.85			2.04
Σ	1.00	0.88	4.26	4.22	5.12	5.11	

Bond-valence parameters are taken from Gagné and Hawthorne (2015).

$^{M(1)}(Ti_{0.67}Sn_{0.33})^{M(2)}(Sn_{0.67}Ti_{0.33})$ (Crennell *et al.*, 1992). Yurgensonite is characterised by similar distribution of species-defining Sn and Ti: $^{M(1)}(Ti_{0.67}Sn_{0.33})^{M(2)}(Sn_{0.64}Ti_{0.36})$ (Table 6), which is confirmed by average interatomic distances: *M*(1)–O = 1.991 and *M*(2)–O = 2.017 Å (Table 7).

A synthetic titanium-free tin analogue of KTA, $KSnOAsO_4$ was reported by Lin *et al.* (1995).

Katiarsite and yurgensonite in the Arsenatnaya fumarole form a continuous solid-solution series almost without gaps (Table 3, Fig. 5). The XRD data for its members with different composition together with data on synthetic KTP-type compounds allow us to conclude that all representatives of this series are isostructural and, thus, the katiarsite–yurgensonite series can be considered to be an isomorphous series. We believe that the *M*(1) site in all members of this series is Ti-dominant whereas the *M*(2) site is characterised by wide variation of the Ti:Sn ratio. The formal border between katiarsite, ideally $KTiO(AsO_4)$, and yurgensonite, ideally $K_2SnTiO_2(AsO_4)_2$, should be at the point with composition $K_2Sn_{0.5}Ti_{1.5}O_2(AsO_4)_2$ [= $K_2(Sn_{0.5}Ti_{0.5}O)(TiO)(AsO_4)_2$]. Real composition of the minerals is more complicated due to the presence of significant amounts of admixed *M* cations, and samples with Sn > 0.5 Sn apfu are considered as corresponding to the mineral species yurgensonite (##9–13 in Table 3).

Iron and antimony are the common substituents in the majority of the samples of katiarsite–yurgensonite series minerals studied (Table 3). It is impossible to quantify the distribution of Fe and Sb between the *M*(1) and *M*(2) sites due to the insufficient amounts of these admixed components and similarity of their X-ray scattering power to Ti and Sn, respectively. We suggest that these cations reside in the structure as Fe^{3+} and Sb^{5+}. This conclusion is based on (1) general crystal chemical features of KTP-type compounds (see above), (2) strongly oxidising conditions of mineral formation in the Arsenatnaya fumarole (Pekov *et al.*, 2018a; Shchipalkina *et al.*, 2020) and (3) the presence of rutile and cassiterite strongly enriched by the tripuhyite component, i.e. Fe^{3+} and Sb^{5+} which together substitute Ti^{4+} (Sandalov *et al.*, 2020), in close association with katiarsite–yurgensonite series members. The substitution scheme with participation of Sb for these KTP-type arsenate minerals seems the same: $Fe^{3+} + Sb^{5+} \rightarrow 2M^{4+}$ (*M* = Sn and Ti). It is noteworthy that the substitution $M^{3+} + M^{5+} \leftrightarrow 2M^{4+}$ is in general typical for KTP-type compounds (Weber, 2003). This is also in agreement with the ionic radii which are (in octahedral coordination) as follows: Sn^{4+} 0.69, Ti^{4+} 0.605, Sb^{5+} 0.60 and Fe^{3+} 0.645 Å whereas ionic radii of Sb^{3+} and Fe^{2+} are 0.76 and 0.78 Å, respectively (Shannon, 1976). However, some samples of minerals of the katiarsite–yurgensonite series exhibit a substantial, up to 0.4 apfu, admixture of Fe+Al (with Fe >> Al), without concomitant incorporation of Sb^{5+} (Table 3). As the presence of Fe^{4+} can be ruled out under natural (terrestrial) oxidation conditions, and neither F^- nor OH^- were detected in the samples of katiarsite and yurgensonite, the sole mechanism which can be invoked for compensation of the emerging charge imbalance is the introduction of oxygen vacancies. The trivalent centres (Fe, Cr, Ti, In and Sc) and associated oxygen vacancies are well-known in both synthetic $KTiOPO_4$ (KTP) and $KTiOAsO_4$ (KTA) (e.g. Bulka *et al.*, 1987; Gaite *et al.*, 1991; Mashkovtsev and Isaenko, 1996). The vacancies arise *via* paired substitution expressed as: $2M^{4+} + O^{2-} \rightarrow 2M^{3+} + \square$. The concentration of trivalent cations in the synthetic samples of KTP and KTA not exceeded 0.0*n* atoms per formula with 5 oxygen atoms, as the laser-grade KTP and KTA are grown as high-purity crystals. If the

https://doi.org/10.1180/mgm.2021.47 Published online by Cambridge University Press

proposed substitution mechanism is also valid for minerals of the katiarsite–yurgensonite series, they might contain up to 0.08 oxygen vacancies per formula with 5 oxygen atoms. This is among the highest vacancy contents ever detected in the compounds belonging to the KTP-structure type.

Acknowledgements. We thank anonymous referees for valuable comments. This study was supported by the Russian Science Foundation, grant no. 19-17-00050. The technical support by the SPbSU X-Ray Diffraction Resource Center in the powder XRD study is acknowledged.

Supplementary material. To view supplementary material for this article, please visit https://doi.org/10.1180/mgm.2021.47

References

Agilent Technologies (2014) *CrysAlisPro Software system, version 1.171.37.35*. Agilent Technologies UK Ltd, Oxford, UK.

Anthony J.W., Bideaux R.A., Bladh K.W. and Nichols M.C. (1990a) *Handbook of Mineralogy, Volume II. Silica, Silicates*. Mineral Data Publishing, Tucson, AZ, 904 pp.

Anthony J.W., Bideaux R.A., Bladh K.W. and Nichols M.C. (1990b) *Handbook of Mineralogy, Volume III. Halides, Hydroxides, Oxides*. Mineral Data Publishing, Tucson, AZ, 628 pp.

Britvin S.N., Dolivo-Dobrovolsky D.V. and Krzhizhanovskaya M.G. (2017) Software for processing the X-ray powder diffraction data obtained from the curved image plate detector of Rigaku RAXIS Rapid II diffractometer. *Zapiski Rossiiskogo Mineralogicheskogo Obshchestva*, **146**, 104–107 [in Russian].

Bulka G.R., Vinokurov V.M., Nizamutdinov N.M. and Khasanova N.M. (1987) Pseudosymmetry of spin-Hamiltonian tensor in coordination polyhedral of Fe^{3+} in $KTiOPO_4$ by EPR data. *Soviet Physics – Crystallography*, **32**, 408–413.

Churakov S.V., Tkachenko S.I., Korzhinskii M.A., Bocharnikov R.E. and Shmulovich K.I. (2000) Evolution of composition of high-temperature fumarolic gases from Kudryavy volcano, Iturup, Kuril Islands: the thermodynamic modeling. *Geochemistry International*, **38**, 436–451.

Crennell S.J., Owen J.J., Cheetham A.K., Kaduk J.A. and Jarman R.H. (1991) A combined X-ray and neutron powder diffraction study of $K(Ti_{½}Sn_{½})OPO_4$. *European Journal of Solid State Inorganic Chemistry*, **28**, 397–407.

Crennell S.J., Cheetham A.K., Kaduk J.A. and Jarman R.H. (1992) Isomorphous substitution in non-linear optical $KTiOPO_4$: Powder diffraction studies of $K_{0.5}Rb_{0.5}SnOPO_4$, $K_{0.5}Na_{0.5}Ti_{0.5}Sn_{0.5}OPO_4$, $Na_{0.5}Rb_{0.5}Ti_{0.5}Sn_{0.5}OPO_4$ and $K_{0.5}Rb_{0.5}Ti_{0.5}Sn_{0.5}OPO_4$. *Journal of Materials Chemistry*, **2**, 785–792.

Gagné O.C. and Hawthorne F.C. (2015) Comprehensive derivation of bond-valence parameters for ion pairs involving oxygen. *Acta Crystallographica*, **B71**, 562–578.

Gaite J.M., Stenger J.F., Dusausoy Y., Marnier G. and Rager H. (1991) Electron paramagnetic resonance study of paramagnetic defect centres Fe^{3+} and Cr^{3+} in $KTiOPO_4$. *Journal of Physics: Condensed Matter*, **3**, 7877–7886.

Krotova O.D., Sorokina N.I., Verin I.A., Voronkova V.I., Yanovskii V.K. and Simonov V.I. (2003) Structure and properties of single crystals of tin-doped potassium titanyl phosphate. *Crystallography Reports*, **48**, 925–932.

Lin K.-J., Lin H.-C. and Lii K.-H. (1995) Synthesis and characterization of $ASnOAsO_4$ (A = K and Rb). *Journal of the Chinese Chemical Society (Taipei)*, **42**, 913–918.

Mashkovtsev R.I. and Isaenko L.I. (1996) Spectroscopic study of $KTiOAsO_4$ single crystals doped with In, Sc, Fe. *Physica Status Solidi*, **B198**, 577–585.

Mayo S.C., Thomas P.A., Teat S.J., Loiacono G.M. and Loiacono D.N. (1994) Structure and nonlinear optical properties of $KTiOAsO_4$. *Acta Crystallographica*, **B50**, 655–662.

Nakamoto K. (1986) *Infrared and Raman Spectra of Inorganic and Coordination Compounds*. John Wiley & Sons, New York.

Nespolo M. and Ferraris G. (2000): Twinning by syngonic and metric merohedry. Analysis, classification and effects on the diffraction pattern. *Zeitschrift für Kristallographie*, **215**, 77–81.

Northrup P.A., Parise J.B., Cheng L.K., Cheng L.T. and McCarron E.M. (1994) High-temperature single-crystal X-ray diffraction studies of potassium and (cesium, potassium) titanyl arsenates. *Chemistry of Materials*, **6**, 434–440.

Novikova N.E., Sorokina N.I., Verin I.A., Alekseeva O.A., Orlova E.I., Voronkova V.I. and Tseitlin M. (2018) Structural reasons for the nonlinear optical properties of KTP family single crystals. *Crystals*, **8**, 283.

Pautov L.A. and Agakhanov A.A. (1997) Berezanskite, $KLi_3Ti_2Si_{12}O_{30}$, a new mineral. *Zapiski Vserossiiskogo Mineralogicheskogo Obshchestva*, **126**, 75–80 [in Russian].

Pekov I.V., Zubkova N.V., Yapaskurt V.O., Belakovskiy D.I., Lykova I.S., Vigasina M.F., Sidorov E.G. and Pushcharovsky D.Yu. (2014a) New arsenate minerals from the Arsenatnaya fumarole, Tolbachik volcano, Kamchatka, Russia. I. Yurmarinite, $Na_7(Fe^{3+},Mg,Cu)_4(AsO_4)_6$. *Mineralogical Magazine*, **78**, 905–917.

Pekov I.V., Zubkova N.V., Yapaskurt V.O., Belakovskiy D.I., Vigasina M.F., Sidorov E.G. and Pushcharovsky D.Yu. (2014b) New arsenate minerals from the Arsenatnaya fumarole, Tolbachik volcano, Kamchatka, Russia. II. Ericlaxmanite and kozyrevskite, two natural modifications of $Cu_4O(AsO_4)_2$. *Mineralogical Magazine*, **78**, 1527–1543.

Pekov I.V., Zubkova N.V., Yapaskurt V.O., Belakovskiy D.I., Vigasina M.F., Sidorov E.G. and Pushcharovsky D.Yu. (2015a) New arsenate minerals from the Arsenatnaya fumarole, Tolbachik volcano, Kamchatka, Russia. III. Popovite, $Cu_5O_2(AsO_4)_2$. *Mineralogical Magazine*, **79**, 133–143.

Pekov I.V., Zubkova N.V., Belakovskiy D.I., Yapaskurt V.O., Vigasina M.F., Sidorov E.G. and Pushcharovsky D.Yu. (2015b) New arsenate minerals from the Arsenatnaya fumarole, Tolbachik volcano, Kamchatka, Russia. IV. Shchurovskyite, $K_2CaCu_6O_2(AsO_4)_4$, and dmisokolovite, $K_3Cu_5AlO_2(AsO_4)_4$. *Mineralogical Magazine*, **79**, 1737–1753.

Pekov I.V., Yapaskurt V.O., Britvin S.N., Zubkova N.V., Vigasina M.F. and Sidorov E.G. (2016a) New arsenate minerals from the Arsenatnaya fumarole, Tolbachik volcano, Kamchatka, Russia. V. Katiarsite, $KTiO(AsO_4)$. *Mineralogical Magazine*, **80**, 639–646.

Pekov I.V., Zubkova N.V., Yapaskurt V.O., Polekhovsky Yu.S., Vigasina M.F., Belakovskiy D.I., Britvin S.N., Sidorov E.G. and Pushcharovsky D.Yu. (2016b) New arsenate minerals from the Arsenatnaya fumarole, Tolbachik volcano, Kamchatka, Russia. VI. Melanarsite, $K_3Cu_7Fe^{3+}O_4(AsO_4)_4$. *Mineralogical Magazine*, **80**, 855–867.

Pekov I.V., Yapaskurt V.O., Belakovskiy D.I., Vigasina M.F., Zubkova N.V. and Sidorov E.G. (2017) New arsenate minerals from the Arsenatnaya fumarole, Tolbachik volcano, Kamchatka, Russia. VII. Pharmazincite, $KZnAsO_4$. *Mineralogical Magazine*, **81**, 1001–1008.

Pekov I.V., Koshlyakova N.N., Zubkova N.V., Lykova I.S., Britvin S.N., Yapaskurt V.O., Agakhanov A.A., Shchipalkina N.V., Turchkova A.G. and Sidorov E.G. (2018a) Fumarolic arsenates – a special type of arsenic mineralization. *European Journal of Mineralogy*, **30**, 305–322.

Pekov I.V., Zubkova N.V., Agakhanov A.A., Yapaskurt V.O., Chukanov N.V., Belakovskiy D.I., Sidorov E.G. and Pushcharovsky D.Yu. (2018b) New arsenate minerals from the Arsenatnaya fumarole, Tolbachik volcano, Kamchatka, Russia. VIII. Arsenowagnerite, $Mg_2(AsO_4)F$. *Mineralogical Magazine*, **82**, 877–888.

Pekov I.V., Zubkova N.V., Agakhanov A.A., Belakovskiy D.I., Vigasina M.F., Yapaskurt V.O., Sidorov E.G., Britvin S.N. and Pushcharovsky D.Y. (2019a) New arsenate minerals from the Arsenatnaya fumarole, Tolbachik volcano, Kamchatka, Russia. IX. Arsenatrotitanite, $NaTiO(AsO_4)$. *Mineralogical Magazine*, **83**, 453–458.

Pekov I.V., Zubkova N.V., Agakhanov A.A., Ksenofontov D.A., Pautov L.A., Sidorov E.G., Britvin S.N., Vigasina M.F. and Pushcharovsky D.Yu. (2019b) New arsenate minerals from the Arsenatnaya fumarole, Tolbachik volcano, Kamchatka, Russia. X. Edtollite, $K_2NaCu_5Fe^{3+}O_2(AsO_4)_4$, and alumoedtollite, $K_2NaCu_5AlO_2(AsO_4)_4$. *Mineralogical Magazine*, **83**, 485–495.

Pekov I.V., Lykova I.S., Yapaskurt V.O., Belakovskiy D.I., Turchkova A.G., Britvin S.N., Sidorov E.G. and Scheidl K.S. (2019c) New arsenate minerals from the Arsenatnaya fumarole, Tolbachik volcano, Kamchatka, Russia. XI. Anatolyite, $Na_6(Ca,Na)(Mg,Fe^{3+})_3Al(AsO_4)_6$. *Mineralogical Magazine*, **83**, 633–638.

Pekov I.V., Lykova I.S., Agakhanov A.A., Belakovskiy D.I., Vigasina M.F., Britvin S.N., Turchkova A.G., Sidorov E.G. and Scheidl K.S. (2019d) New arsenate minerals from the Arsenatnaya fumarole, Tolbachik volcano,

Kamchatka, Russia. XII. Zubkovaite, $Ca_3Cu_3(AsO_4)_4$. *Mineralogical Magazine*, **83**, 879–886.

Pekov I.V., Zubkova N.V., Agakhanov A.A., Yapaskurt V.O., Belakovskiy D.I., Vigasina M.F., Britvin S.N., Turchkova A.G., Sidorov E.G. and Pushcharovsky D.Y. (2019e) Yurgensonite, IMA 2019-059. CNMNC Newsletter No. 52; *Mineralogical Magazine*, **83**, 887–893, https://doi.org/10.1180/mgm.2019.73

Pekov I.V., Zubkova N.V., Koshlyakova N.N., Agakhanov A.A., Belakovskiy D.I., Vigasina M.F., Yapaskurt V.O., Britvin S.N., Turchkova A.G., Sidorov E.G., Pushcharovsky D.Y. (2020a) New arsenate minerals from the Arsenatnaya fumarole, Tolbachik volcano, Kamchatka, Russia. XIII. Pansnerite, $K_3Na_3Fe_6^{3+}(AsO_4)_8$. *Mineralogical Magazine*, **84**, 143–151.

Pekov I.V., Koshlyakova N.N., Agakhanov A.A., Zubkova N.V., Belakovskiy D.I., Vigasina M.F., Turchkova A.G., Sidorov E.G., Pushcharovsky D.Yu. (2020b) New arsenate minerals from the Arsenatnaya fumarole, Tolbachik volcano, Kamchatka, Russia. XIV. Badalovite, $NaNaMg(MgFe^{3+})(AsO_4)_3$, a member of the alluaudite group. *Mineralogical Magazine*, **84**, 616–622.

Pekov I.V., Koshlyakova N.N., Agakhanov A.A., Zubkova N.V., Belakovskiy D.I., Vigasina M.F., Turchkova A.G., Sidorov E.G. and Pushcharovsky D.Yu. (2021) New arsenate minerals from the Arsenatnaya fumarole, Tolbachik volcano, Kamchatka, Russia. XV. Calciojohillerite, $NaCaMgMg_2(AsO_4)_3$, a member of the alluaudite group. *Mineralogical Magazine*, **85**, 215–223.

Phillips M.L.F., Harrison W.T.A., Stucky G.D., McCarron III E.M., Calabrese J.C. and Gier T.E. (1992) Effects of substitution chemistry of in the $KTiOPO_4$ structure field. *Chemistry of Materials*, **4**, 222–233.

Sandalov F.D., Pekov I.V., Koshlyakova N.N., Yapaskurt V.O., Agakhanov A.A., Sidorov E.G. and Britvin S.N. (2020) Rutile enriched with chalcophile elements (Sb, Sn, Te) and Ti-rich varieties of tripuhyute and cassiterite from sublimates of active fumaroles at the Tolbachik volcano (Kamchatka, Russia). *Zapiski Rossiiskogo Mineralogicheskogo Obshchestva*, **149**, 22–41 [in Russian].

Shannon R.D. (1976) Revised effective ionic radii and systematic studies of interatomic distances in halides and chalcogenides. *Acta Crystallographica*, **A32**, 751–767.

Shchipalkina N.V., Pekov I.V., Koshlyakova N.N., Britvin S.N., Zubkova N.V., Varlamov D.A. and Sidorov E.G. (2020) Unusual silicate mineralization in fumarolic sublimates of the Tolbachik volcano, Kamchatka, Russia – Part 1: Neso-, cyclo-, ino- and phyllosilicates. *European Journal of Mineralogy*, **32**, 101–119.

Stucky G.D., Phillips M.L.F. and Gier T.E. (1989) The potassium titanyl phosphate structure field: a model for new nonlinear optical materials. *Chemistry of Materials*, **1**, 492–509.

Watson G.H. (1991) Polarized Raman spectra of $KTiOAsO_4$ and isomorphic nonlinear-optical crystals. *Journal of Raman Spectroscopy*, **22**, 705–713.

Weber M.J. (editor) (2003) *Handbook of Optical Materials*. CRC Press, Boca Raton, Florida, USA.

Zelenski M., Malik N. and Taran Yu. (2014) Emissions of trace elements during the 2012–2013 effusive eruption of Tolbachik volcano, Kamchatka: enrichment factors, partition coefficients and aerosol contribution. *Journal of Volcanology and Geothermal Research*, **285**, 136–149.

https://doi.org/10.1180/mgm.2021.47 Published online by Cambridge University Press